Available online at www.sciencedirect.com

SciVerse ScienceDirect

Journal of the European Ceramic Society 32 (2012) 965–973

www.elsevier.com/locate/jeurceramsoc

A route for the pressureless liquid-phase sintering of SiC with low additive content for improved sliding-wear resistance

A.L. Ortiz [a,*], O. Borrero-López [a], M.Z. Quadir [b], F. Guiberteau [a]

[a] Departamento de Ingeniería Mecánica, Energética y de los Materiales, Universidad de Extremadura, 06006 Badajoz, Spain
[b] Electron Microscope Unit, University of New South Wales, Sydney, NSW 2052, Australia

Received 24 August 2011; received in revised form 18 October 2011; accepted 29 October 2011
Available online 3 December 2011

Abstract

A colloidal processing route has been developed for the pressureless sintering of dense SiC with a low content of sintering additives. In this route, a sol–gel solution precursor of the sintering additives is deposited onto the surface of the SiC particles, achieving a uniform distribution of the sintering additives in the green compact. This in turn promotes complete densification at short sintering times, which is not otherwise achievable when the batch is prepared by the standard method of mechanically mixing powders. It is also shown that the resulting ceramic has improved sliding-wear resistance compared to its counterpart prepared by the classical method, with essentially the same rate of mild and severe wear but a notably delayed transition from the mild to the severe wear regimes. This improvement is attributed to the reduction in the microstructural defect size achieved by the colloidal processing. Implications for the fabrication of low-cost SiC ceramics for wear-resistance applications are discussed.

Keyword: SiC; Sintering; Sol-gel processes; Wear resistance

1. Introduction

Silicon carbide (SiC) is one of the ultra-hard ceramics of great attraction for use in tribological applications where resistance to sliding-contacts is required, as for example in bearings, wear-parts, valves, and seals. Apart from its extreme hardness surpassed only by a few compounds, SiC also possesses high chemical stability and thermal conductivity, and an elevated melting point[1–5] that help it to alleviate and resist the frictional heating in sliding-contact applications better than other triboceramics.[6]

Historically, SiC has been solid-state sintered by hot-pressing at high temperatures, but this is not often practical due to its high cost, the brittleness of the resulting ceramics, and the difficulty of fabricating complex shapes without extensive and tedious machining tasks. More commonly, SiC has been solid-state sintered without the application of external pressure with the help of small amounts of B and C,[7] but this is still a costly high-temperature sintering also resulting in brittle ceramics. Pressureless liquid-phase sintering of SiC with metal-oxide additives (generally combinations of aluminium oxide and rare-earth oxides[2,8–13]) does not suffer from these shortcomings, and in addition allows tougher SiC ceramics to be obtained. It is not surprising therefore that the microstructural design of the pressureless liquid-phase-sintered (PLPS) SiC ceramics for tribological applications is an area of particular interest for research. The motivation is that the wear resistance of polycrystalline ceramics is controlled by their average microstructural characteristics.[14] In this context, it is now recognized that the sliding-wear resistance of PLPS SiC ceramics increases significantly with decreasing content of sintering additives,[15,16] the softest ingredient in the microstructure, so that reducing this content as much as possible has emerged as an important processing guideline for wear-resistance applications.[15,16] However, at low volume fractions of liquid phase, complete densification simply by particle rearrangement and pore filling is not possible,[17,18] and prolonged sintering is required to activate extensively the processes of solution-precipitation and grain shape accommodation. However, while this approach may result in full densification, it also promotes grain growth and softening of the intergranular phase,[19] two undesirable consequences in tribological applications because the sliding-wear

* Corresponding author. Tel.: +34 924289600x86726; fax: +34 924289601.
E-mail address: alortiz@materiales.unex.es (A.L. Ortiz).

0955-2219/$ – see front matter © 2011 Elsevier Ltd. All rights reserved.
doi:10.1016/j.jeurceramsoc.2011.10.052

resistance decreases with increasing grain size and with decreasing hardness.[14] Thus, there emerges a dilemma regarding the selection of the optimal sintering conditions, and a compromise is normally reached between the content of sintering additives and the sintering time.

The obtaining of fine-grained PLPS SiC ceramics with low contents of sintering additives thus seems to be a processing challenge beyond the possibilities of the standard method of bath preparation involving the classical mechanical mixture of powders. In this context, we report here a colloidal route of batch preparation to process dense PLPS SiC ceramics with low loads of sintering additives using short sintering times, and demonstrate that the resulting ceramics have improved sliding-wear resistance compared to the PLPS SiC ceramics processed using the conventional method. For this proof-of-concept study, we chose the commonest sintering additive for SiC, the combination $5Al_2O_3 + 3Y_2O_3$ to form $Y_3Al_5O_{12}$ (YAG).

2. Experimental procedure

2.1. Processing

A powder batch was prepared by colloidal processing from a commercially available submicrometre α-SiC (UF-15, H.C. Starck, Germany) powder and a home-made precursor sol–gel solution of YAG obtained in turn from two sol–gel solutions, one rich in Al and the other in Y. The Al-rich solution was prepared by first dissolving 11.4 cm^3 of aluminium s-butoxide (i.e., $Al(OC_4H_9)_3$; 13044, Alfa Aesar, UK) in 115 cm^3 of 2-propanol (i.e., $CH_3CHOHCH_3$; 141090, Panreac, Spain) plus 5.7 cm^3 of nitric acid 69% (i.e., HNO_3; 141037, Panreac, Spain), followed by stirring for 3 h. This solution was then hydrolyzed with 1.7 cm^3 of distilled water, and stirred for 2 h. The Y-rich solution was prepared similarly from 9 g of yttrium acetate (i.e., $Y(OOCCH_3)_3{\cdot}4H_2O$; 14565, Alfa Aesar, Spain), 115 cm^3 of 2-propanol, and 6.7 cm^3 of nitric acid, but with no water since the alkoxide contains enough water for the hydrolysis. The individual Al- and Y-rich solutions were then mixed together, and stirred for 2 h. Subsequently, 95 g of the α-SiC powder was added and the suspension was stirred for 2 h, after which the slurry was dried under stirring. The resulting powder (hereafter referred to as colloidal SiC powder) was dried in an oven at 100 °C for 48 h to remove the water and part of the organics, and was de-agglomerated by crushing and sieved through a 20-μm sieve. Note that the chemical composition of the colloidal powder was designed to yield a PLPS SiC ceramic with 96.4 vol.% SiC and 3.6 vol.% YAG after sintering.

A reference powder batch was also prepared from the classical mechanical mixture of powders (hereafter referred to as conventional SiC powder). In particular, 95 g of the same α-SiC powder was mixed with 2.15 g of Al_2O_3 (AKP-30, Sumitomo Chemical Company, USA) and 2.85 g of Y_2O_3 (Fine-Grade, H.C. Starck, Germany) powders, which were then blended intimately by wet-ball-milling in methanol for 24 h. The same steps described above of slurry and powder drying, de-agglomeration, and sieving were also carried out in this case. The conventional powder was also designed to result in a PLPS SiC ceramic with 96.4 vol.% SiC and 3.6 vol.% YAG after sintering.

From each of the powder batches, compacts were made by uniaxial pressing (C, Carver Inc., USA) at 50 MPa, followed by isostatic pressing (CP360, AIP, USA) at 350 MPa. Next, individual pellets were embedded in loose powder beds composed of 90 wt% SiC (600 grit; Crystolon, Norton Co., USA) and 10 wt% Al_2O_3 (15 μm, Buehler, Ltd., USA) inside graphite crucibles with screw lids, and were then pressureless sintered. This pressureless sintering was performed in a graphite furnace (1000-3560-FP20, Thermal Technology Inc., USA) at 1950 °C for 1 h in a flowing Ar-gas atmosphere of 99.999% purity, with heating and cooling rates of 600 and 1200 °C h^{-1}, respectively. The sintered ceramics (hereafter referred as to colloidal and conventional PLPS SiC ceramics) were cleaned and ground down 1 mm to remove the layer of adhered powder bed, and their densities were measured using the Archimedes method with distilled water as the immersion medium.

2.2. Microstructural characterization

The powder batches were analyzed using various characterization techniques, as needed – in particular, X-ray diffractometry (XRD) for the identification of the amorphous or crystalline nature of the phases present, scanning and transmission electron microscopy (SEM and TEM, respectively) for the direct examination of the size and morphology of the powder particles, N_2-adsorption isotherms for the measurement of the specific surface area, and X-ray photoemission spectroscopy (XPS) for the determination of the surface composition and bonding environment or status. The XRD patterns were collected in step-scanning mode (step width 0.02° 2θ, angular range 29–51° 2θ, and count time 3 s/step) using a high-resolution laboratory diffractometer (D8 Advance, Bruker AXS, Germany) equipped with a primary monochromator that provides pure Cu$K\alpha_1$ radiation (λ = 1.54056 Å) and a linear ultra-fast detector; the phases present in the XRD patterns were identified with the aid of the PDF2 database. The SEM observations were done at 20 kV with backscattered electrons, using a field-emission gun microscope (S-4800II, Hitachi, Japan). The TEM observations were made at 200 kV in bright-field mode, also using a field-emission gun microscope (CM200, Philips, The Netherlands). The N_2-adsorption isotherms were acquired at −196 °C using a Sievert volumetric gas sorption analyzer (Autosorb-1, Quantachrome Instruments, UK), and the specific surface area was calculated using the Brunauer–Emmett–Teller equation. The XPS spectra were recorded in ultra-high vacuum (10^{-6} Pa) using a high-resolution spectrometer (K-Alpha, Thermo Scientific) equipped with a monochromatic Al-Kα X-ray source (1486.6 eV), and making two types of measurement: (1) a survey scan in the 0–1350 eV range at 1 eV resolution, and (2) detailed scans in the 63–83 and 148–163 eV ranges at 0.05 eV energy resolution, which correspond to the Al 2p and Y 3d core lines respectively. The protocol of sample preparation for each of these techniques followed standard procedures for ceramic powders.

The colloidal and conventional PLPS SiC ceramics were characterized by XRD as described above (step width 0.02°

2θ, angular range 26–48° 2θ, and count time 3 s/step), and also by scanning electron microscopy (S-3600N, Hitachi, Japan). For the SEM observations, cross-sections of the two PLPS SiC ceramics were ground and polished to a 1-μm finish using routine ceramographic methods. The polished specimens were then plasma-etched (PT 1750, Fissions Instruments, East Sussex, UK) for 2 h using CF_4-4%O_2 gas to reveal the microstructure, and were observed with secondary electrons at 20 kV. The average grain size and the average size of the microstructural defects in each ceramic were quantified by image analysis (AnalySIS, Olympus Soft Imaging Solutions GmbH, Germany) using various SEM micrographs taken randomly.

2.3. Sliding-wear testing

Several polished disks (7 mm diameter, 2 mm thickness) were core-drilled from the colloidal and conventional PLPS SiC ceramics for the wear testing. Sliding-wear testing was performed at room temperature using a multi-specimen tribometer (Falex, Faville-Le Vally Corp., USA) configured in the ball-on-three-disks geometry. In this testing configuration a commercial, bearing grade Si_3N_4 ball (NBD 200, Cerbec, USA) of radius 6.35 mm is rotated in contact with three flat disk specimens aligned with their surface normals in tetrahedral coordination relative to the rotation axis and mounted onto a bearing assembly to ensure equal distribution of the applied load. Paraffin oil (Heavy Grade, Fisher Scientific, USA) with a viscosity of $\sim 3.4 \times 10^{-5}$ m^2/s (~34 cst) at 40 °C was used as the lubricant to avoid any tribological effects such as friction-induced heating or tribo-reactions. The contact load was 210 N and the rotation speed was 100 rpm, corresponding to a sliding velocity of ~0.04 m/s. The wear tests were interrupted at intervals, and the diameters of the circular wear scars on each disk were measured under optical microscopy (two orthogonal measurements per disk, three disks per PLPS SiC ceramic). After each interruption the specimens were put back in the tribometer in exactly the same position using a precision fixture. The wear-scar diameter was used to quantify the extent of wear damage. Finally, the wear damage was observed under SEM.

Conventional Vickers indentation tests (MV-1, Matsuzawa, Japan) were performed to evaluate the hardness and toughness of the two PLPS SiC ceramics. The tests were performed with 98 N load (5 indentations per ceramic), and the hardness and toughness values were determined using the standard procedure and formulas.[20,21]

3. Results and discussion

3.1. Processing

Fig. 1 compares the XRD patterns of the as-received and colloidal SiC powders. There are certain similarities and certain differences in the XRD patterns after the colloidal processing, which provide insights into its effects on the SiC powder. Firstly, no additional peaks appeared, which rules out the precipitation of new crystalline phases (such as Al_2O_3, Y_2O_3, YAG or any other mixed oxide of Y and Al). Secondly, the background level

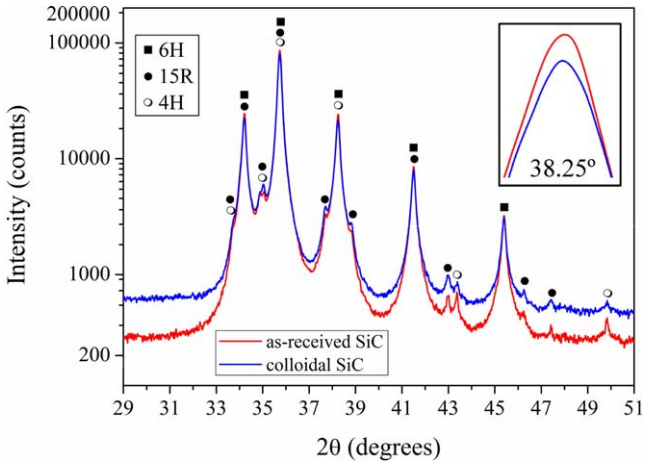

Fig. 1. XRD patterns of the SiC powders before and after the colloidal processing. The phase identification is included. The logarithmic scale of the *Y*-axis is to facilitate the appreciation of the weakest peaks. The inset shows in more detail the phenomenon of attenuation of the SiC signal (note again the logarithmic scale on the *Y*-axis).

increased, which reveals the existence of diffuse scattering from an amorphous phase. Thirdly, the SiC peaks remained in place, which excludes the formation of solid solutions with Al, Y, and/or O atoms as solutes in the SiC host. This is consistent with the fact that no Al, Y, or O inward diffusion is expected to occur in SiC at the drying temperature of 100 °C. And fourthly, the intensity of the SiC peaks decreased notably, which is clear evidence that something attenuates the SiC signal. Taken together, all these observations indicate that the sol–gel solution has coated the surface of the SiC particles with an amorphous film composed of heavy elements (such as Y and Al, and also O). The XRD pattern of the conventional SiC powder (not shown) was as expected, simply with the SiC, Y_2O_3, and Al_2O_3 peaks.

The specific surface area of the SiC powder was found to decrease from 13.75 $m^2\,g^{-1}$ in the as-received condition to 13.08 $m^2\,g^{-1}$ after the colloidal processing. Although the equivalent particle diameter cannot be measured from the specific surface area because the SiC particles have a complex shape (see the TEM micrograph of Fig. 2), which precludes further quantitative analysis, it can at least be inferred that the colloidal processing leads to the SiC particles becoming slightly larger. Since particle growth is clearly impossible in loose SiC powder at the drying temperature of 100 °C, as was also confirmed by heat-treating the as-received powder at 100 °C for 48 h, this increase in the particle size necessarily reflects the presence of a nanometric-thick film on the surface of the SiC particles. Thus, the N_2-adsorption analysis is entirely consistent with the XRD analysis.

The examination of the colloidal SiC powder by electron microscopy provides the direct evidence confirming the clear conclusion[a] already inferred from the XRD and N_2-adsorption analyses that the sol–gel solution coated the surface of the SiC

[a] Note that the information obtained by XRD and N_2-adsorption is very representative in statistical terms because the typical XRD and N_2-adsorption experiments analyze various millions of particles.

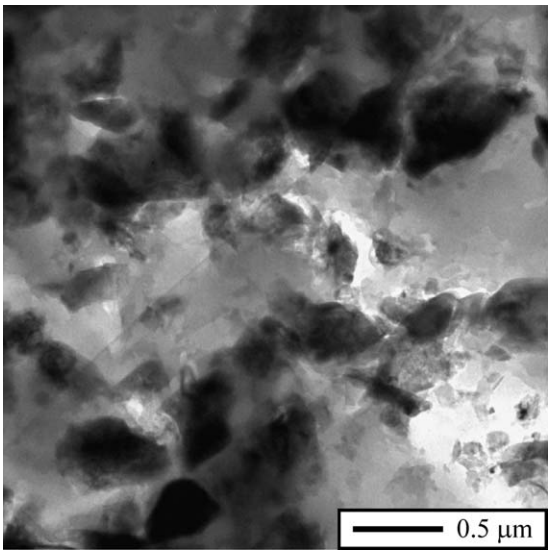

Fig. 2. Bright-field low-magnification TEM image of the SiC powder particles in the as-received condition, showing the irregular shape of the particles.

particles. Thus, not only did the extensive SEM observations in backscattered-electron mode not reveal the presence of Al- or Y-rich individual particles, but the detailed TEM observations such as the one presented in Fig. 3 showed clearly the existence of a nano-film with ∼5 nm thickness on the surface of the SiC particles. This nano-film is believed to be rich in Al, Y, and O, something that will be investigated by XPS instead of energy dispersive X-ray spectrometry (EDS) in the TEM. This is because, while the spatial resolution of the XPS and EDS techniques is similar (i.e., ∼10 nm), XPS has better energy resolution and the chemical shifts in the XPS spectra provide information on the binding state of the elements present. Fig. 4 shows the survey XPS spectrum of the colloidal SiC powder. It is clear that the surface nano-film on the SiC particles is composed of Al, Y, and

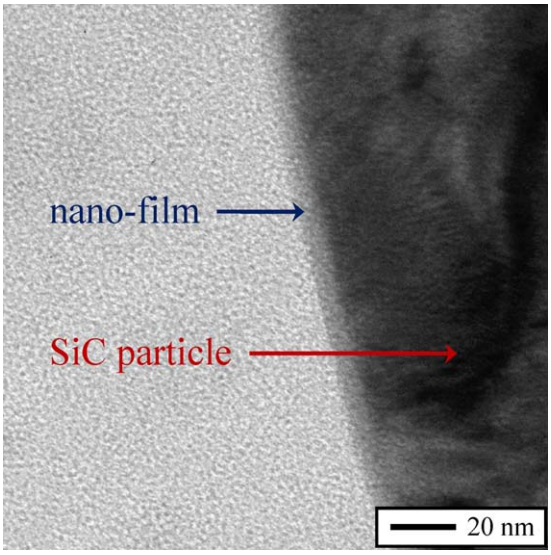

Fig. 3. Bright-field high-magnification TEM image of the SiC powder particles after the colloidal processing, showing the presence of a nano-film on the surface of the SiC particles.

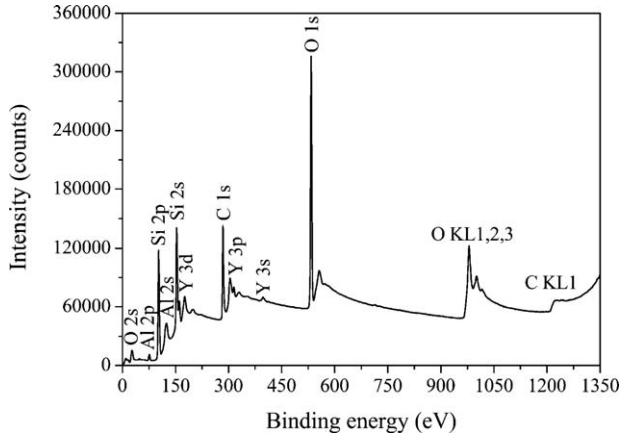

Fig. 4. Survey XPS spectrum of the SiC powder after the colloidal processing. Also included in the figure is the peak indexing, including the Auger peaks.

O because, as was mentioned above, the observation of the Si and C peaks is due simply to the limited spatial resolution of the XPS analysis. It can also be seen in the detailed XPS spectra of the Al 2p and Y 3d core levels shown in Fig. 5 that both peaks are quite broad, which is due to the combination of the following two factors: (1) the well-known spin-orbit interaction of these

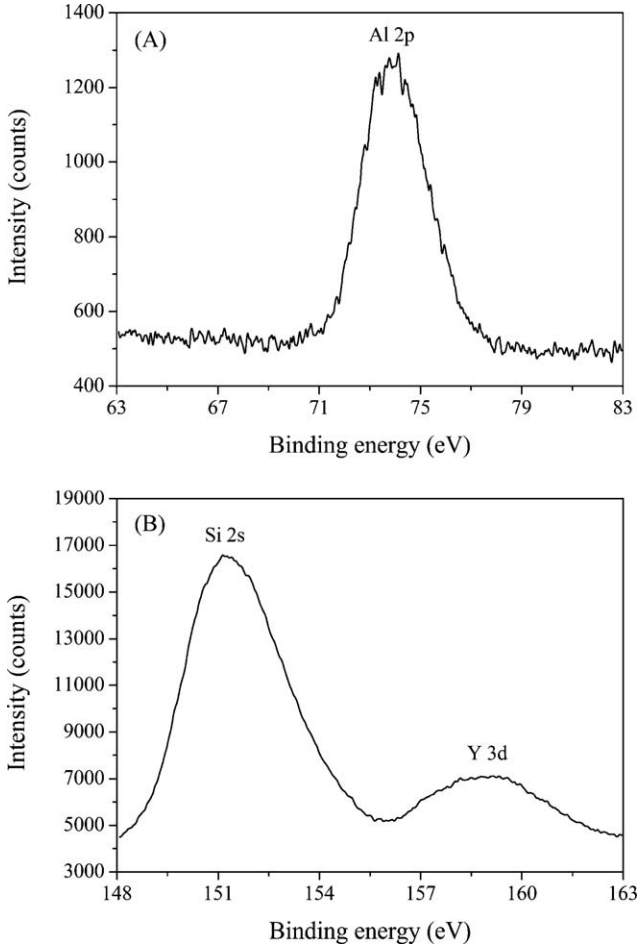

Fig. 5. High-resolution XPS spectra of the Al 2p (doublet Al $2p_{3/2}$–$2p_{1/2}$) and Y 3d (doublet Y $3d_{5/2}$–$3d_{3/2}$) core-levels for the SiC powder after the colloidal processing.

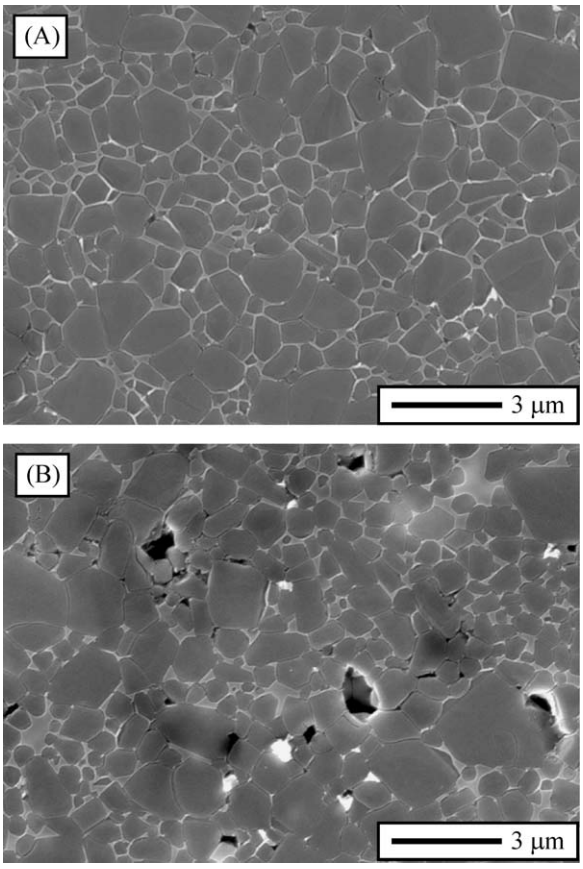

Fig. 6. SEM micrographs of the polished and plasma-etched cross-sections of the (A) colloidal PLPS SiC ceramic and (B) conventional PLPS SiC ceramic.

lines (i.e., the doublets Al $2p_{3/2}$–$2p_{1/2}$ and Y $3d_{5/2}$–$3d_{3/2}$, respectively), and (2) the amorphous nature of the nano-film structure, as was also inferred from the XRD analysis. One also observes in Fig. 5 that the Al 2p peak is located at a binding energy of ~73.9 eV, which is higher than the ~73.0 eV reported for Al[22] and than the ~73.4 eV reported for Al_2O_3.[23] Similarly, the Y 3d peak is located at a binding energy of ~158.9 eV, which is much higher than the ~155.7 eV reported for Y[24] and than the ~156.7 eV reported for Y_2O_3.[24] Such high binding energies of the Al 2p and Y 3d core levels have, however, been observed in the corresponding metal hydroxides, [23,25] which reveals that the oxide nano-film deposited on the surface of the SiC particles has at this stage the amorphous structure of a wet gel with the Y and Al atoms being connected through oxo and hydroxo bridges.

Fig. 6 compares representative SEM micrographs of the two PLPS SiC ceramics. As can be observed, both exhibit the expected microstructure, that is, SiC grains with secondary phase located mostly at triple junctions of the grain structure. It can also be seen that the two microstructures are similar in terms of the size and morphology of the SiC grains. Thus, in both cases the SiC grains are equiaxed with the same aspect ratio of 1.4, which is the equilibrium shape of α-SiC,[26] and are fine with the same average size of ~0.6 μm, which is only 0.1 μm greater than the particle size of the as-received SiC powder. However, it can also be seen in Fig. 6 that the microstructure of the colloidal PLPS SiC ceramic is clearly more

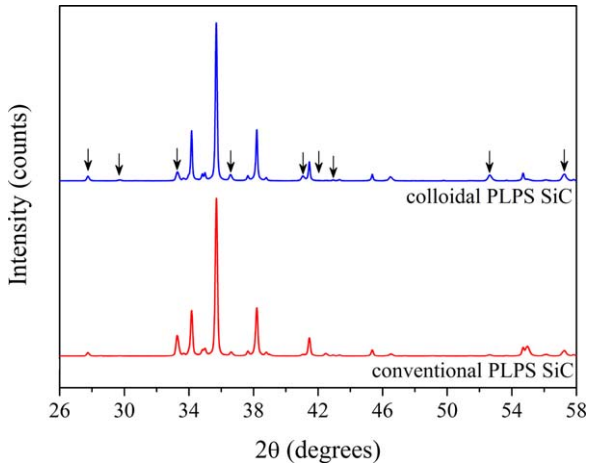

Fig. 7. XRD patterns of the colloidal and conventional PLPS SiC ceramics. The arrows indicate the YAG peaks. The indexing of the rest of the peaks (not included) is as shown in Fig. 1. The XRD patterns have been shifted along the *Y*-axis to facilitate the comparison.

homogeneous, that is, with a much more uniform distribution of the intergranular phase between the SiC grains as there is no evidence of the large intergranular-phase pockets or of the porous regions that are observed in the conventional PLPS SiC ceramic. Indeed, the density measurements by the Archimedes method confirmed that the colloidal PLPS SiC ceramic is fully dense, whereas the conventional PLPS SiC ceramic has ~5% residual porosity. Nevertheless, the detailed examination of the SEM micrograph in Fig. 6A reveals the presence of few grain-facet flaws of ~0.2 μm in average size, much smaller than the pores of ~1 μm in Fig. 6B.

The XRD analysis of the two PLPS SiC ceramics reveals that their phase composition is similar. As can be seen in Fig. 7, both contain the 6H, 15R, and 4H polytypes of SiC already present in the as-received powder, plus the new YAG phase. This indicates that according to the chemical composition of the powder batches, during sintering the Y_2O_3 and Al_2O_3 in the conventional PLPS SiC ceramic reacted to form YAG, whereas the Y and Al metal hydroxides in the colloidal PLPS SiC ceramic completed the polycondensation reaction to produce YAG.

3.2. Sliding wear

Fig. 8 compares the sliding-wear curves of the two PLPS SiC ceramics. It can be seen that the evolution of the wear-scar size with the sliding time is qualitatively similar for the two materials, i.e., the wear scar first increases slowly, and then abruptly after a certain sliding time. Furthermore, these two-stretch curves are of the same shape as the wear curves typical of other polycrystalline ceramics,[14,27–30] from which it can be inferred that the cumulative material removal during the sliding wear of both PLPS SiC ceramics also occurred by two successive mechanisms: dislocation plasticity with little material loss (i.e., mild wear), followed by fracture with extensive material loss (i.e., severe wear). The important feature to note in Fig. 8 is that transition from the mild-wear regime to the severe-wear regime occurred ~2.5-times later in the colloidal PLPS SiC ceramic

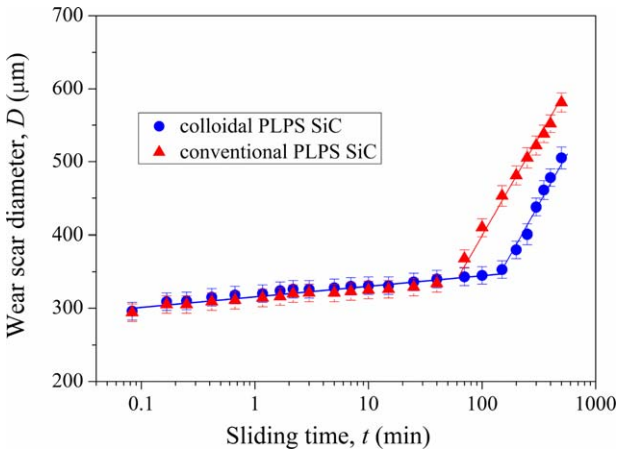

Fig. 8. Wear curves – wear scar diameter as a function of the sliding time on a logarithmic scale – for the colloidal and conventional PLPS SiC ceramics. Each datum point is the mean of three specimens tested; error bars represent data dispersion. The solid lines are fits to the data, with the discontinuities in the lines indicating the mild-to-severe wear transition.

(i.e., at 150 vs 70 min), which is a clear indication of greater wear resistance. The two PLPS SiC ceramics have, however, within the experimental errors, the same rates of mild and severe wear, that is, 14.5 and 283.5 μm/log t, respectively, as determined by fitting the empirical expression $A + B \log t$ to the experimental data of D vs log t in each wear regime.

The observations of the post-transition wear scars presented in Fig. 9 corroborate the lesser susceptibility of the colloidal PLPS SiC ceramic to severe surface degradation. Thus, while these micrographs show that the type of damage is the same in the two materials, in particular, grooves and scratches at the macroscopic scale and grain boundary fracture and grain pullout at the microstructure scale, they also show that the damage is less pronounced in the colloidal PLPS SiC ceramic (smaller size of the wear scar and lower density of grooves in its interior, as well as fewer grain pullouts).

Finally, the hardness and toughness measured by Vickers testing were 23.1 ± 0.3 GPa and 3.3 ± 0.3 MPa $m^{0.5}$ for the colloidal PLPS SiC ceramic, and 22.8 ± 0.3 GPa and 3.6 ± 0.2 MPa $m^{0.5}$ for the conventional PLPS SiC ceramic. The two materials thus have essentially the same hardness and toughness: the slight difference is due simply to the former being fully dense, whereas the latter has ~5% residual porosity.

4. Analysis

We have presented a new colloidal route of SiC batch preparation, and demonstrated that it is especially useful for the fabrication of dense PLPS SiC ceramics with low contents of sintering additives. Essentially, this new route involves the preparation of a concentrated suspension of SiC particles in a liquid precursor solution of the oxide additives (YAG in the present case) prepared previously by the sol–gel method, followed by drying the suspension under stirring to promote the deposition of a metal-oxide nano-film onto the surface of the SiC particles. The attractiveness of this colloidal processing route is that it leads to a better dispersion of minimal contents of sintering additives. Thus, whereas in the compacts made from powder batches prepared by the classical mechanical mixture of powders the sintering additives are discretely dispersed as submicrometre-sized

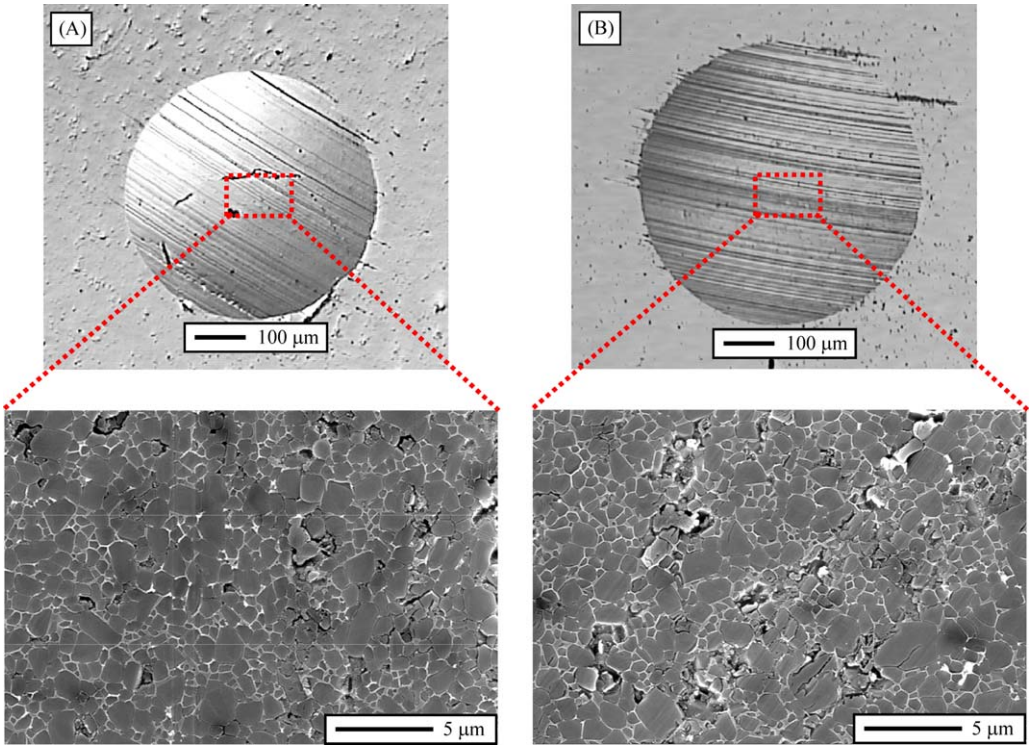

Fig. 9. Micrographs of the damage after 500 min of sliding wear (end of the wear tests) at the macroscopic (optical) and microstructural (SEM) levels in the (A) colloidal PLPS SiC ceramic and (B) conventional PLPS SiC ceramic.

particles between the SiC particles, in those prepared colloidally they are continuously distributed because the surface of each SiC particle has been engineered chemically to carry a nano-film of the sintering additives, as was demonstrated by XRD (Fig. 1), N_2-adsorption, TEM (Fig. 3), and XPS (Fig. 4). This nano-film has initially the amorphous structure of a wet gel as identified by XRD (Fig. 1) and XPS (Fig. 5) because the drying temperature of only 100 °C is insufficient to complete the reaction of polycondensation, which nevertheless occurs in the very early stages of the heating ramp (<300 °C) during the sintering heat treatment. Note that this does not represent any obstacle to the subsequent densification because at these low temperatures the porous nature of the compact facilitates the escape of the volatile residues generated. Indeed, this scenario is actually preferred over the introduction of an additional step of powder calcination prior to the compaction, not only because of the simplification of the processing routine, but also because the calcination is likely to result in the formation of hard agglomerates due to the hot-welding of the SiC particles through their oxide nano-film, and the resulting agglomerated powders have proven to be difficult to sinter.[18] Eventually, the oxypolymer resulting from the polycondensation reaction forms crystalline YAG at higher temperatures during the heating ramp, as confirmed by XRD (Fig. 7).

The better dispersion of the sintering additives achieved with the colloidal processing is essential to reach full densification together with a homogeneous microstructure. This becomes clear in Fig. 6, which shows that, whereas the colloidal PLPS SiC ceramic is fully dense (Fig. 6A), the conventional PLPS SiC ceramic has ~5% porosity under the same sintering conditions (Fig. 6B). To explain these observations we will consider some basic aspects of sintering theory in the presence of a small volume fraction of liquid. It is well-known that once the liquid phase has formed, the solid particles re-pack to a higher coordination, a phenomenon known as particle rearrangement which helps densification.[17,18] Simultaneously, the liquid formed flows preferentially into the nearest pores, while also wetting the neighbouring particles. This generates an attractive capillary force that tends to bring the particles together, increasing in magnitude as the separation between particles decreases.[17,18] The result is to enhance the densification not only directly, but also indirectly as liquid is released that is available to fill other pores. Despite these phenomena occurring in both PLPS SiC ceramics, there are some fundamental differences between them. In particular, in the colloidal PLPS SiC ceramic the liquid phase forms homogeneously at the surface of each SiC particle, so all of them undergo rearrangement and wetting thus leading to a better particle packing with a smaller pore size. On the contrary, in the conventional PLPS SiC ceramic the liquid phase formation occurs locally because the liquid forms at the additive particle site, so the particle wetting and the rearrangement densification is somewhat more limited. The smaller pore size in the colloidal PLPS SiC ceramic implies that less liquid is needed to fill a given pore, and therefore there is more liquid available to fill other pores. Its better particle wetting and packing imply greater capillary forces, which in turn result in the release of a greater amount of liquid to be redistributed for the filling of pores. In addition, in the colloidal PLPS SiC ceramic the pore filling is more effective simply because of its shorter spreading distance. All these differences reinforce each other in enhancing the densification in the colloidal PLPS SiC ceramic relative to the conventional PLPS SiC ceramic.

Apart from the events just described, further densification occurs in the two PLPS SiC ceramics during sintering when the grain-shape accommodation induced by the solution-reprecipitation mechanism starts to contribute to the pore elimination,[17,18] which in turn also contributes to releasing liquid that is available to fill remaining pores. Overall, these processes are also much more effective in the colloidal PLPS SiC ceramic due to its better packing with smaller pore size, its homogeneous distribution of liquid, and its shorter spreading distance. Note that all this is especially relevant in the present case because the sintering lasted only 1 h in order to avoid grain growth and softening of the intergranular phase[19] that would otherwise have been detrimental to the sliding-wear resistance,[14] whose improvement is the objective pursued here.

We have also demonstrated that the colloidal PLPS SiC ceramic is more resistant to sliding wear than the conventional PLPS SiC ceramic because, while both have the same rates of mild and severe wear, the former enters the severe-wear regime much later. This enhancement in the wear resistance can be explained using the simple mechanistic model developed earlier for the sliding wear of non-transforming polycrystalline ceramics.[27] This model posits that, during the mild-wear regime, plastic-deformation damage is introduced within the different phases, inducing tensile stresses (σ_D) that bear up against the grain boundaries and accumulate as a function of the sliding time t. In two-phase ceramics, such as the PLPS SiC ceramics, these stresses are added to the material's internal residual tensile stresses (q) which are independent of the sliding time.[b] The time-dependent stress intensity factor ($K(t)$) acting on the pre-existing defects under the wear contact is given by

$$K(t) = \psi(\sigma_D(t) + q)L^{0.5}$$

where ψ is a crack-geometry coefficient and L is the defect size. At a certain critical sliding time (t_c) the stress intensity factor at defects will reach the grain-boundary toughness (K_{GB})

$$K(t_c) = \psi(\sigma_D(t_c) + q)L^{0.5} = K_{GB}$$

at which moment grain-boundary fracture and subsequent grain pullout take place, representing the onset of the transition from mild deformation wear to severe fracture wear.

[b] These stresses arise from the thermal expansion mismatch, and are given by[31,32]:

$$q = V(1-V)E\Delta T\Delta\alpha$$

where V is the volume fraction of the second phase, E the average elastic modulus of the composite, ΔT the temperature range through which the composite is cooled without stress relaxation, and $\Delta\alpha$ the thermal expansion mismatch. Using $\Delta\alpha \sim 5\times10^{-6}\,°C^{-1}$ for the thermal expansion mismatch between SiC and YAG, $E \sim 410$ MPa, $\Delta T \sim 1500$ °C, and $V = 0.036$, q is calculated to be 53 MPa. This is valid for both the colloidal and the conventional PLPS SiC ceramics.

With this background, consider first the similarity in the mild-wear rate of the two PLPS SiC ceramics. This is reasonable because mild wear is controlled by dislocation plasticity, and is therefore dictated by the hardness which is nearly the same for the two materials. In this scenario the rates at which the plasticity-induced stresses accumulate within the SiC grains and YAG phase are the same in the two PLPS SiC ceramics, thus explaining the similarity observed experimentally for the slope of the mild-wear regime.

Consider now the timing for the wear-regime transition. For a situation such as the present one, in which there are no differences in the rate at which the plasticity-induced stresses accumulate, in the grain-boundary toughness, or in the internal residual stress,[c] the model simply establishes an inverse relationship between wear-stage transition time and the square root of the size of the pre-existing defects: $t_c \propto L^{-0.5}$. The way in which the additives were introduced during processing is then of critical importance because the SEM microstructural observations showed that the average defect size is only ~0.2 μm in the colloidal PLPS SiC ceramic (grain-facet flaws in Fig. 6A), but ~1 μm in the conventional PLPS SiC ceramic (pores in Fig. 6B). This 5-fold reduction in the defect size achieved by the colloidal processing predicts a 2.24-fold increase in the wear-regime transition time, which is in perfect agreement with the experimental measurement (i.e., a 2.14-fold increase).

Consider finally the similarity in the severe-wear rate of the two PLPS SiC ceramics. This is also reasonable because the material removal in this wear regime occurs by grain pullout due to grain-boundary fracture and also by abrasion by third bodies (i.e., the wear debris) trapped under the contact during sliding. The fracture is affected by the toughness, which is nearly the same for the two materials. The rate of abrasive wear caused by sharp third bodies is a complex function that depends on the abraded material through the factor $K_{IC}^{-0.5}H^{-1.425}$, and also on the hardness of the abrasives. The factor $K_{IC}^{-0.5}H^{-1.425}$ is the same within experimental error for the two ceramics, as is the hardness of the abrasives because in both the wear debris contains statistically the same fraction of SiC and YAG. Given that there are no large differences in either of these two mechanisms (fracture or abrasion), the net result is the similar rate of severe wear of the two PLPS SiC ceramics that is observed experimentally in Fig. 8.

The present study has therefore presented clear experimental evidence that the introduction of low loads of sintering additives by colloidal processing with sol–gel solutions is an effective approach for making PLPS SiC ceramics more wear resistant, which can be added to the existing list of processing guidelines.[15,16,33–36] The results also have interesting implications because they suggest that there is still room for further reductions in the content of sintering additives and relaxation of the sintering conditions (time and perhaps temperature), with the consequent doubly beneficial impact that this would have on the wear resistance. If successful, this would pave the way for the pressureless sintering of nanostructured SiC ceramics with minimal additive contents, a long sought for objective. Furthermore, the intimate mixture of the reactants at the atomic scale achieved by the colloidal processing with sol–gel solutions would allow both the currently used and new additive compositions to be prepared with the fine chemical control difficult to attain with the classical mixture of powders. The confluence of all these factors represents an unprecedented opportunity for creating a next-generation of low-cost SiC ceramics for wear-resistance applications. Exploring this possibility, however, remains for future work.

[c] The rate of plasticity-induced stress accumulation is the same because the wear tests in Fig. 8 revealed no differences in the slope of the mild-wear regime. The grain-boundary toughness is the same because it depends on the chemistry of the grain/matrix interfaces, which is SiC/YAG in both cases. Finally, the internal residual stresses were computed to be 53 MPa in both cases.

5. Concluding remarks

We have presented a colloidal processing route especially suitable for the pressureless liquid-phase sintering of dense SiC with a low sintering additive content. Essentially, this route entails covering the surface of each SiC particle in the powder with a nano-film of a sol–gel solution that is a precursor of the sintering additives. The uniform distribution of the sintering additives in the green compact achieved in this way promotes complete densification at short sintering times, which is not attainable when the batch is prepared by the standard method of mechanical mixture of powders. We have also demonstrated that this enhancement in densification provides the resulting ceramics with superior sliding-wear resistance, in particular with a delayed transition from the mild to the severe wear regime. Based on the experimental results and analyses, it emerges that the proposed colloidal processing is an effective approach for making PLPS SiC ceramics more wear resistant. Finally, we have discussed the broad implications that this new colloidal processing may have for the fabrication of a next-generation of low-cost SiC ceramics for wear-resistance applications.

Acknowledgements

The authors thank Drs. R. Caruso (CONICET-UNR, Argentina) and A. Díaz-Parralejo (University of Extremadura, Spain) for assistance with the preparation of the sol–gel solution. This work was supported by the Ministerio de Ciencia y Tecnología (Government of Spain) under Grant No. MAT 2010-16848.

References

[1]. Meetham GW, Van de Voorde MH. *Materials for high temperature engineering applications*. New York: Springer; 2000.

[2]. Padture NP. *In situ*-toughened silicon carbide. *J Am Ceram Soc* 1994;**77**(2):519–23.

[3]. Zum Gahr K-H, Blattner R, Hwang D-H, Pöhlmann K. Micro- and macro-tribological properties of SiC ceramics in sliding contact. *Wear* 2001;**250**(1–12):299–310.

[4]. Sigl LS. Thermal conductivity of liquid phase sintered silicon carbide. *J Eur Ceram Soc* 2003;**23**(7):1115–22.

[5]. Schlesinger ME. Melting points, crystallographic transformation and thermodynamic values. In: Schneider SJ, editor. *Engineered materials handbook*, vol. 4. ASM International; 1991. p. 883–91.
[6]. Bhushan B. *Modern tribology handbook*. New York: CRC Press; 2001.
[7]. Prochazka S, Scanlan RM. Effect of boron and carbon on sintering of SiC. *J Am Ceram Soc* 1975;**58**(1–2):72.
[8]. Cordrey L, Niesz DE, Shanefield DJ. Sintering of silicon carbide with rare-earth oxide additives. In: Handwerker CA, Blendell JE, Kaysser WA, editors. *Ceramic transactions*, vol. 7. Westerville, OH: Sintering of Advanced Ceramics, American Ceramic Society; 1990. p. 618–36.
[9]. Pujar VV, Jensen RP, Padture NP. Densification of liquid-phase-sintered silicon carbide. *J Mater Sci Lett* 2000;**19**(11):1011–4.
[10]. Sigl LS, Kleebe H-J. Core/rim structure of liquid-phase-sintered silicon carbide. *J Am Ceram Soc* 1993;**76**(3):773–6.
[11]. Zhou Y, Hirao K, Toriyama M, Yamauchi Y, Kanzaki S. Effect of intergranular phase chemistry on the microstructure and mechanical properties of silicon carbide ceramics densified with rare-earth oxide and alumina additives. *J Am Ceram Soc* 2001;**84**(7):1642–4.
[12]. Rodríguez-Rojas F, Ortiz AL, Guiberteau F, Nygren M. Oxidation behaviour of pressureless liquid-phase-sintered α-SiC with additions of $5Al_2O_3 + 3RE_2O_3$ (RE = La, Nd, Y, Er, Tm, or Yb). *J Eur Ceram Soc* 2010;**30**(15):3209–17.
[13]. Rodríguez-Rojas F, Ortiz AL, Guiberteau F, Nygren M. Anomalous oxidation behaviour of pressureless liquid-phase-sintered SiC. *J Eur Ceram Soc* 2011;**31**(13):2393–400.
[14]. Wang X, Padture NP, Tanaka H, Ortiz AL. Wear-resistant ultra-fine-grained ceramics. *Acta Mater* 2005;**53**(2):271–7.
[15]. Borrero-López O, Ortiz AL, Guiberteau F, Padture NP. Effect of microstructure on sliding-wear properties of liquid-phase-sintered α-SiC. *J Am Ceram Soc* 2005;**88**(8):2159–63.
[16]. Borrero-López O, Ortiz AL, Guiberteau F, Padture NP. Microstructural design of sliding-wear-resistant liquid-phase-sintered SiC: an overview. *J Eur Ceram Soc* 2007;**27**(11):3351–7.
[17]. German RM. *Liquid phase sintering*. New York, US: Plenum Press; 1985.
[18]. German RM. *Sintering theory and practice*. New York, US: John Willey and Sons; 1996.
[19]. Borrero-López O, Pajares A, Ortiz AL, Guiberteau F. Hardness degradation in liquid-phase-sintered SiC with prolonged sintering. *J Eur Ceram Soc* 2007;**27**(11):3359–64.
[20]. Green DJ. *An introduction to the mechanical properties of ceramics*. Cambridge, UK: Cambridge University Press; 1998.
[21]. Anstis GR, Chantikul P, Marshall DB, Lawn BR. A critical evaluation of indentation techniques for measuring fracture toughness: I. Direct crack measurements. *J Am Ceram Soc* 1981;**64**(9):533–8.
[22]. Nylund A, Olefjord I. Surface analysis of oxidized aluminium 1. Hydration of Al_2O_3 and decomposition of $Al(OH)_3$ in a vacuum as studied by ESCA. *Surf Interface Anal* 1994;**21**(5):283–9.
[23]. Thomas S, Sherwood PMA. Valence band spectra of aluminum oxides, hydroxides, and oxyhydroxides interpreted by X.alpha calculations. *Anal Chem* 1992;**64**(21):2488–95.
[24]. Briggs D, Seah MP. *Practical surface analysis: by Auger and X-ray photoelectron spectroscopy*. New York, US: John Willey and Sons; 1983.
[25]. Barr TL. An ESCA study of the termination of the passivation of elemental metals. *J Phys Chem* 1978;**82**(16):1801–10.
[26]. Xu H, Bhatia T, Deshpande SA, Padture NP, Ortiz AL, Cumbrera FL. Microstructural evolution in liquid-phase-sintered SiC: part I, effect of starting powder. *J Am Ceram Soc* 2001;**21**(9):1578–84.
[27]. Cho S-J, Hockey BJ, Lawn BR, Bennison SJ. Grain-size and *R*-curve effects in the abrasive wear of alumina. *J Am Ceram Soc* 1989;**72**(7):1249–52.
[28]. Cho S-J, Moon H, Hockey BJ, Hsu SM. The transition from mild to severe wear in alumina during sliding. *Acta Metall Mater* 1992;**40**(1):185–92.
[29]. Wang YS, Hsu SM. Wear and wear transition mechanisms of ceramics. *Wear* 1996;**195**(1–2):112–22.
[30]. Thompson SC, Pandit A, Padture NP, Suresh S. Stepwise-graded Si_3N_4–SiC ceramics with improved wear properties. *J Am Ceram Soc* 2002;**85**(8):2059–64.
[31]. Lawn BR, Padture NP, Braun LM, Bennison SJ. Model for toughness curves in 2-phase ceramics. 1. Basic fracture-mechanics. *J Am Ceram Soc* 1993;**76**(9):2235–40.
[32]. Padture NP, Runyan JL, Bennison SJ, Braun LM, Lawn BR. Model for toughness curves in 2-phase ceramics. 2. Microstructural variables. *J Am Ceram Soc* 1993;**76**(9):2241–7.
[33]. Borrero-López O, Ortiz AL, Guiberteau F, Padture NP. Improved sliding-wear resistance in *in-situ* toughened silicon carbide. *J Am Ceram Soc* 2005;**88**(12):3531–4.
[34]. Borrero-López O, Ortiz AL, Guiberteau F, Padture NP. Sliding-wear-resistant liquid-phase sintered SiC processed using α-SiC starting powders. *J Am Ceram Soc* 2007;**90**(2):541–5.
[35]. Borrero-López O, Ortiz AL, Guiberteau F, Padture NP. Effect of the nature of the intergranular phase on sliding-wear resistance of liquid-phase-sintered α-SiC. *Scr Mater* 2007;**57**(6):505–8.
[36]. Ciudad E, Borrero-López O, Rodríguez-Rojas F, Ortiz AL, Guiberteau F. Effect of intergranular phase chemistry on the sliding-wear resistance of pressureless liquid-phase-sintered α-SiC. *J Eur Ceram Soc* 2012;**32**(2):511–6.